1. Feedback From The First Stars

Once the first stars reach the main sequence, they will have a profound effect on their environment. Their high lumosity and hot T_{eff} means they emit more and harder UV flux than similar mass Solar metallicity stars. They will ionize the surrounding gas. As the number of first stars increases in a given halo, the reoinization of the baryonic matter proceeds outward within the halo. The escape of ionizing radiation from early galaxies with luminous stars and quasars requires assuming a detailed description of the density of the gas in 3D (clumping being important) as well as that of the first stars within the halo; detailed calculations are necessary. The escape fraction determined for local starburst galaxies is $\sim 20\%$, but may be lower in high redshift galaxies, when the Universe was much denser ($\rho \propto (1+z)^3$).

Another issue to bear in mind when calculating the reionization of the halo gas from a luminous first star is that because the density of the IGM at high redshifts is high, recombinations (rate $\propto n_H^2$) cannot be ignored. This reduces the efficiency of reionization below that naively expected.

Reionization of He from HeI to HeII is also expected given the high T_{eff} (hard ionizing spectrum) characteristic of first stars. There is enough radiation at $\lambda < 24.6$ eV, the ionization threshold of HeI, to do that, but reionization to fully ionized He requires an additional 54 eV, and so that will take longer to occur. Note that Lyα absorption by HeII occurs at 304 Å, and has been detected in a small number of intermediate redshift QSOs with HST spectroscopy.

In studying reonization, one must avoid the proximity effect, a region near the QSO itself where the gas has been blown out, the density is low, and hence the ionization is higher than at regions far enough from the QSO that local effects are not relevant.

At the end of the reionization stage, an intense UV background fills the Universe and heats the IGM to $T \sim 20,000$ K. Photoionization of the denser collapsed gas with $T_{vir} < 10,000$ K then proceeds, and may heat the gas enough to evaporate it back into the IGM.

When the massive first stars stars die, the input of energy from their SN explosions into the halo gas may produce shocks, and strong outflows. These shocks may then become sites for additional subsequent star formation, while if the gas is heated and dispersed, star formation will be halted. Evidence for large scale outflows ("galactic winds") in local group starbursting dwarfs has been detected through extended soft X-ray emission and imaging diffuse emission in Hα; see, e.g. *Properties of Galactic Outflows: Measurements of theFeedback from Star Formation*, C. Martin, 1999, ApJ, 513, 156. Does this hot gas fall back into the proto-galaxy or does it escape ? The balance between outflows and accretion affects the reservoir of gas available for star formation.

Furthermore, the nuclear processed material within the first stellar generation is eventually dispersed by either very large mass loss through stellar winds or by SN explosions. This leads to dispersal of elements heavier than those produced in the Big Bang (H, He, Li, Be) into the surrounding gas and eventually throughout the halo, enriching the gas to eventally reach the critical metallicity where cooling by metals is important, and thus to end the phase of 0Z star formation.

All of these processes are local around particular first stars. The gas is not reionized all at the same time, nor are the SN synchronized, so reionization and dispersal of heavy elements are local processes and do not occur instantaeously for all gas in a particular halo at a specific redshift z_{rein}.

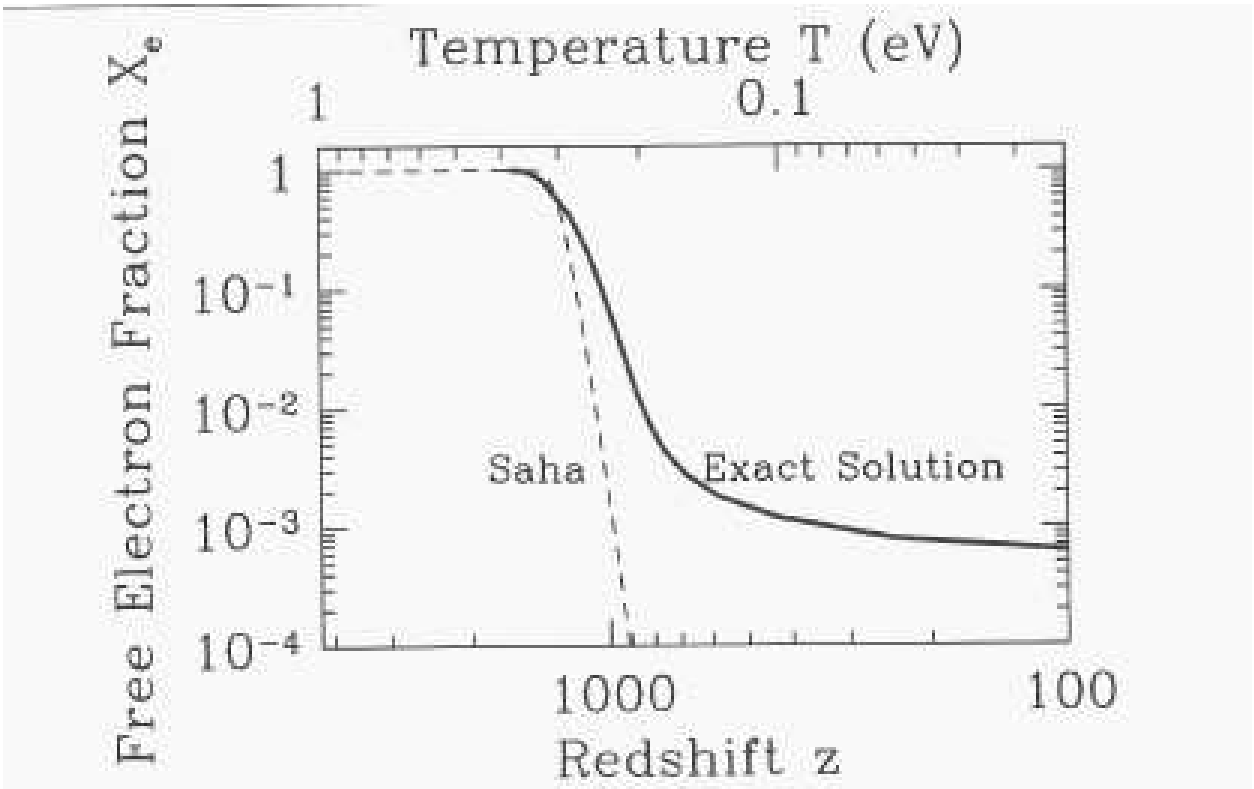

Figure 3.4. Free electron fraction as a function of redshift. Recombination takes place suddenly at $z \sim 1000$ corresponding to $T \sim 1/4$ eV. The Saha approximation, Eq. (3.37), holds in equilibrium and correctly identifies the redshift of recombination, but not the detailed evolution of X_e. Here $\Omega_b = 0.06, \Omega_m = 1, h = 0.5$.

Fig. 1.— Fig. 3-4 from Dodelson, *Modern Cosmology*.

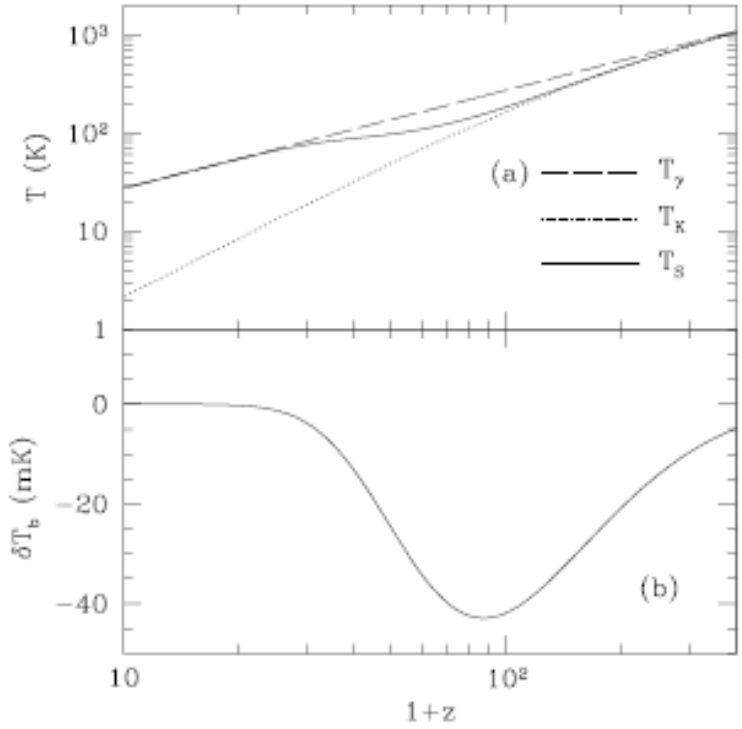

Fig. 6. *(a)*: IGM temperature evolution if only adiabatic cooling and Compton heating are involved. The spin temperature T_S includes only collisional coupling. *(b)*: Differential brightness temperature against the CMB for T_S shown in panel *a*.

Fig. 2.— IGM temperature evolution ignoring star formation and stellar energy input into the IGM. The lower panel is the differential brightness temperature of T_S, the hydrogen spin temperature, which determines the strength of the (reshifted) 21 cm line, against the CMB. (Fig. 6 from Furlanetto, Peng Oh & Briggs, 2006, Phys. Reports, 433, 181, a lengthly review *Cosmology at Low Frequencies: The 21 cm Tranisition and the High Redshift Universe.*

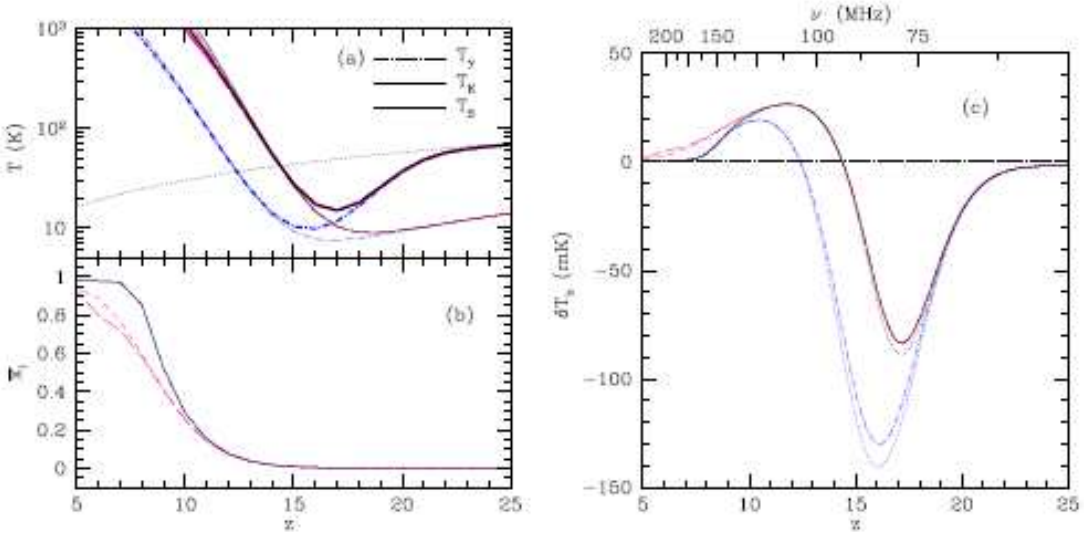

Fig. 7. Global IGM histories for Pop II stars. The solid curves take our fiducial parameters without feedback. The dot-dashed curve takes $f_X = 0.2$. The short- and long-dashed curves include strong photoheating feedback. *(a)*: Thermal properties. *(b)*: Ionized fraction. *(c)*: Differential brightness temperature against the CMB. In this panel, the two dotted lines show δT_b without including shock heating. From [270].

Fig. 3.— IGM temperature evolution including star formation and stellar energy input into the IGM. The right panel is the differential brightness temperature of T_S, the hydrogen spin temperature, which determines the strength of the (reshifted) 21 cm line, against the CMB. (Fig. 7 from Furlanetto, Peng Oh & Briggs, 2006, Phys. Reports, 433, 181.)

1.1. Reionization of the Gas

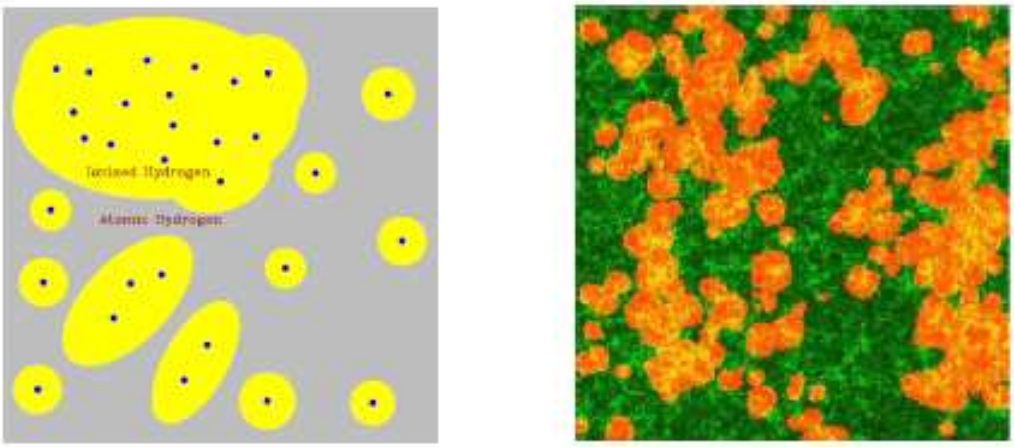

Fig. 4. The spatial structure of cosmic reionization. The illustration (left panel, based on Barkana & Loeb 2004b) shows how regions with large-scale overdensities form large concentrations of galaxies (dots) whose ionizing photons produce enormous joint ionized bubbles (upper left). At the same time, galaxies are rare within large-scale voids, in which the IGM is still mostly neutral (lower right). A numerical simulation of reionization (right panel, from Mellema et al. 2006) indeed displays such variation in the sizes of ionized bubbles (orange), shown overlayed on the density distribution (green).

Fig. 4.— Fig. 4 of Loeb, 2007, Astro-ph:0711.3463, lecture for "Astrophysics in the Next Decade"

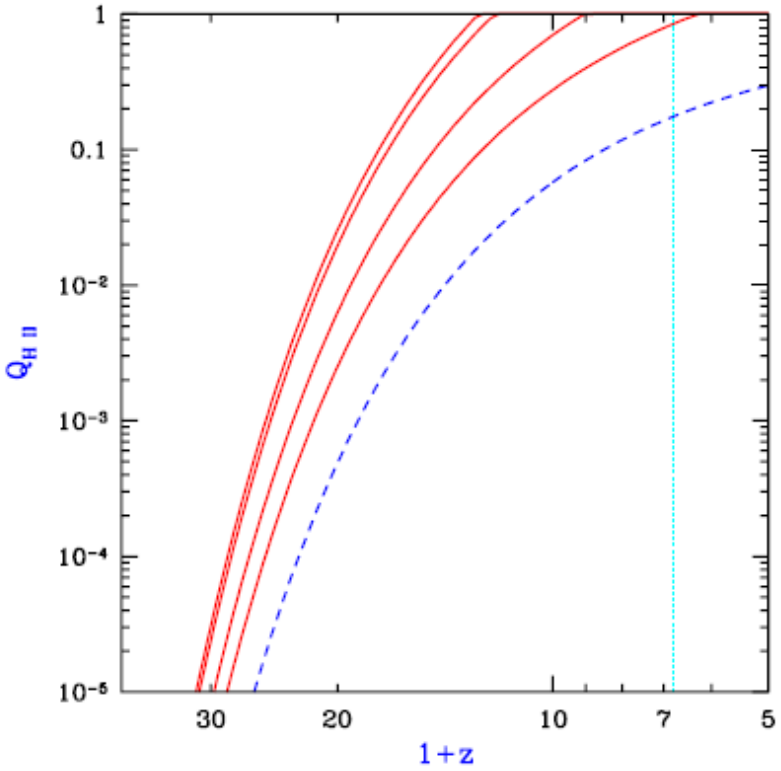

Fig. 22.— Semi-analytic calculation of the reionization of the IGM (for $N_{\rm ion} = 40$), showing the redshift evolution of the filling factor $Q_{\rm H\ II}$. Solid curves show $Q_{\rm H\ II}$ for a clumping factor $C = 0$ (no recombinations), $C = 1$, $C = 10$, and $C = 30$, in order from left to right. The dashed curve shows the collapse fraction $F_{\rm coll}$, and the vertical dotted line shows the $z = 5.8$ observational lower limit (Fan et al. 2000) on the reionization redshift.

Fig. 5.— Fig. 22 from Barkana & Loeb, 2001.

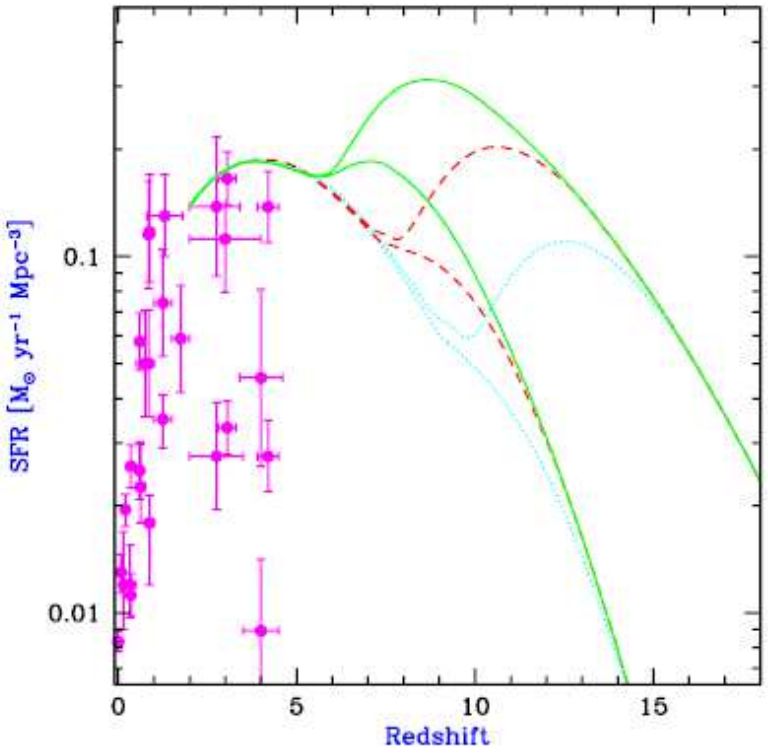

Fig. 29.— Redshift evolution of the SFR (in $M_\odot$ per year per comoving Mpc^3), adopted from Figure 1 of Barkana & Loeb (2000b) with slight modifications. Points with error bars are observational estimates (compiled by Blain et al. 1999a). Also shown are model predictions for a reionization redshift $z_{\rm reion} = 6$ (solid curves), $z_{\rm reion} = 8$ (dashed curves), and $z_{\rm reion} = 10$ (dotted curves), with a star formation efficiency $\eta = 10\%$. In each pair of curves, the upper one is the total SFR, and the lower one is the fraction detectable with *NGST* at a limiting point source flux of 0.25 nJy. We assume the ΛCDM model (with parameters given at the end of §1).

Fig. 6.— Fig. 29 from Barkana & Loeb, 2001.

1.2. Relevant Observations

Direct detection of the epoch of reionization:

a) Gunn-Peterson effect in QSOs – SDSS discovery of high redshift QSOs ($z \sim 6$). SDSS cannot find higher redshift QSOs due to limited range of spectrum covered by the filters used, a near=IR extension to the SDSS would be required. Note that the constraints imposed by non-detection of any radiation below the Lyman limit at typical observational uncertainties characteristic of faint, high redshift QSOs, are not very strong; an effective optical depth of $\tau \sim 5$ at $z \sim 6$ in the HI Lyα forest does not imply that reonization is occuring because the absorption saturates for neutral fractions of $\sim 10^{-5}$. The main observational challenge is determining the level of the Lyman continuum at emitted $\lambda < 912$ Å. Furthermore a detailed model of the IGM, including the voids, where the optical depth will be very low, and of the UV radiation field as a function of redshift is required. (see, e.g. Becker, Rauch & Sargent, 2007, ApJ, 662, 72)

Note that in the appended figures from this paper there is no abrupt change in the degree of ionization between $2 < z < 6$.

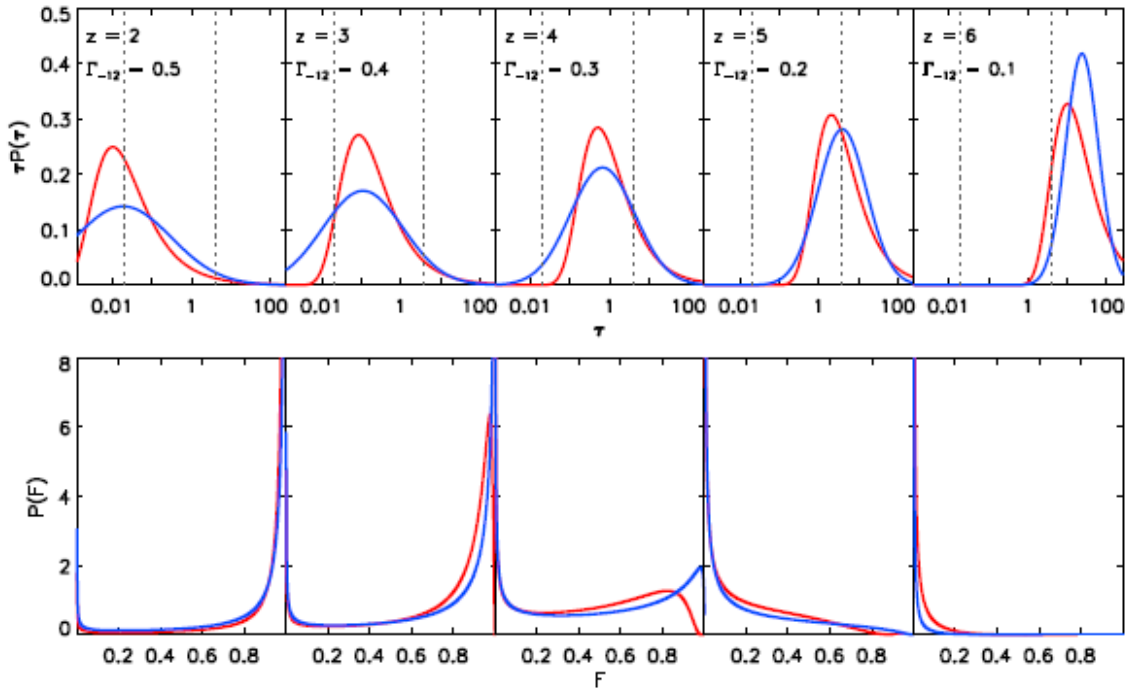

Fig. 11.— Redshift evolution of the theoretical Lyα optical depth and transmitted flux distributions. The top panels show the τ distributions for the indicated redshifts and ionization rates. Bottom panels show the corresponding transmitted flux PDFs. Distributions for the MHR00 model are shown in red. Distributions for the lognormal τ model are shown in blue. Parameters for the lognormal τ distribution were calculated from fits to μ and σ as a function of redshift (cf. equations 10 and 11). Vertical dotted lines indicate optical depths corresponding to 98% and 2% transmitted flux. The clearest differences in the predicted *shapes* of the flux PDFs occur at $3 < z < 5$. The lognormal τ distribution, which produces better fits to the data, narrows with redshift more rapidly than the MHR00 τ distribution. Hence, fewer pixels with measurable transmitted flux at $z = 6$ are predicted in the lognormal case.

Fig. 7.— Fig. 11 of Becker, Rauch & Sargent, 2007, ApJ, 662, 72 *The Evolution of optical depth in the Lyα Forest: evidence against reionization at* $z \sim 6$. Two models for the optical depth distribution are considered, their lognormal model and a commonly-used model for the IGM density by Miralda-Escude, Haehnelt & Rees (2000, ApJ, 530, 1). Top panels - distribution of optical depth in Lyα. Bottom panel - probability distribution function for the transmitted flux at Lyα. The models must represent the IGM including voids, groups, galaxy clusters, etc.

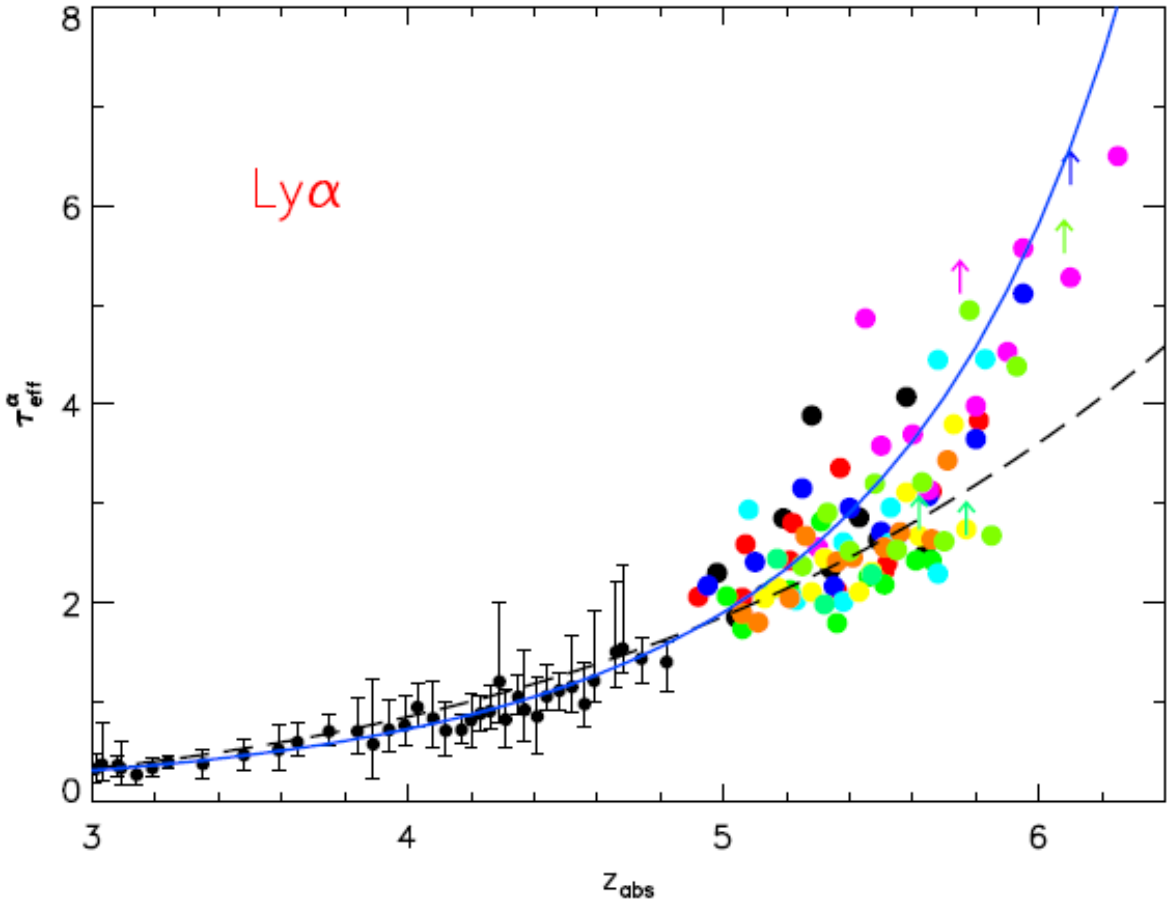

Fig. 12.— The evolution of Lyα effective optical depth with redshift, where $\tau_{\rm eff} = -\ln\langle F\rangle$. Data points are from Songaila (2004) (small circles) and Fan et al. (2006) (large circles and arrows, with colors matching their Figure 2). The dashed line shows the best-fit power-law to $\tau^{\alpha}_{\rm eff}$ at $z < 5.5$ from Fan et al. (2006). The solid line shows $\tau^{\alpha}_{\rm eff}$ calculated from the lognormal distribution of Lyα optical depths, for which the parameters were fit at $z < 5.4$. A simple evolution in the lognormal τ distribution predicts the upturn in $\tau^{\alpha}_{\rm eff}$ at $z > 5.5$ and produces a better fit to the observed $\tau^{\alpha}_{\rm eff}$ at $4 < z < 5$.

Fig. 8.— The mean optical depth at Lyα as a function of redshift. When the IGM is neutral, it is large, but as the First Stars reionize the iGM, τ becomes smaller. Fig. 12 of Becker, Rauch & Sargent, 2007, ApJ, 662, 72.

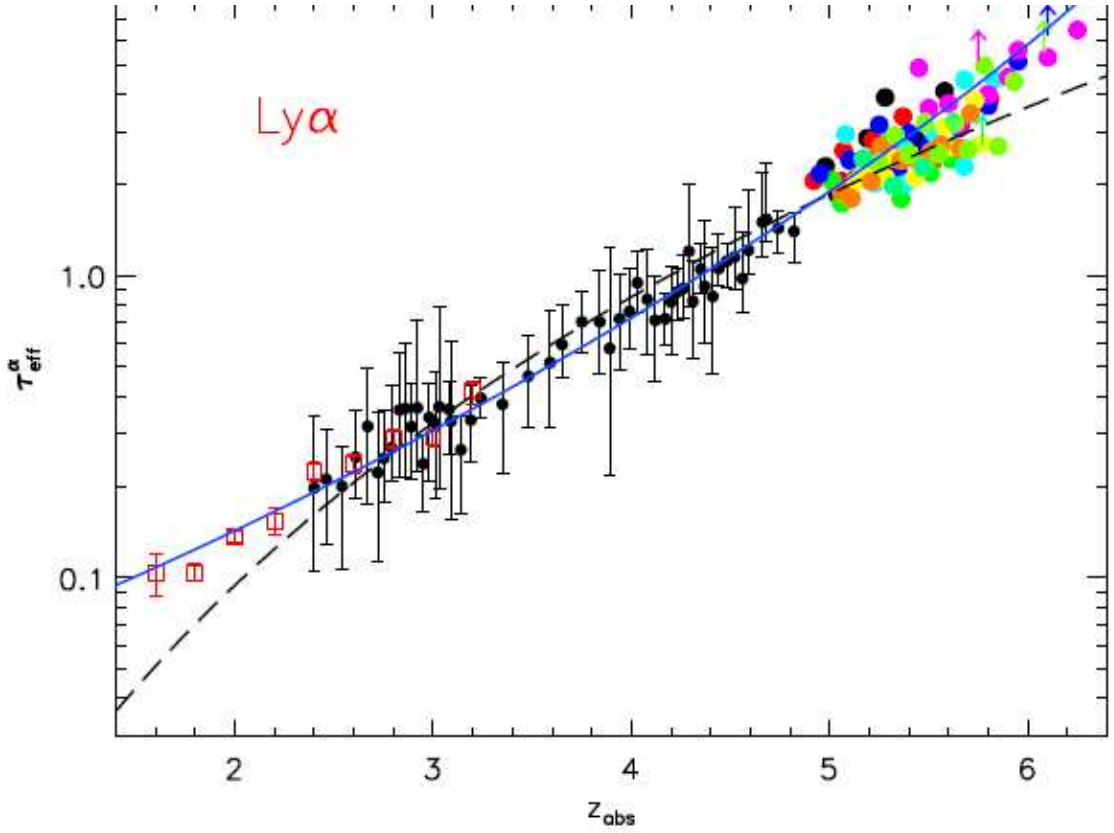

Fig. 13.— Same as Figure 12, with $\tau^{\alpha}_{\rm eff}$ on a logarithmic scale. We have also included lower-redshift measurements calculated from Kirkman et al. (2005), which exclude absorption from metal lines, Lyman limit systems, and damped Lyα systems. The Kirkman et al. (2005) points are plotted as open squares with errors in the mean measurements. The power-law fit from Fan et al. (2006) (dashed line) under-predicts the amount of Lyα absorption both at $z > 5.7$ and at $z < 2.5$. In contrast, $\tau^{\alpha}_{\rm eff}$ calculated from the lognormal τ distribution (solid line), provides a simultaneously good fit to all points at $1.6 < z < 6.2$.

Fig. 9.— Fig. 13 of Becker, Rauch & Sargent, 2007, ApJ, 662, 72.

b) A new perspective on the epoch of reionization perhaps can be obtained using GRBs to reach higher redshift. The prompt X-ray and γ-ray emission of GRBs is not attenuated by gas or dust, and hence GRBs should in principle be detected from the reionization era. Furthermore GRBs at maximum are very luminous, and their intrinsic emission, ignoring absorption from the IGM, is featureless, unlike QSOs. This requires an X-ray satellite to detect the GRB, ideally something more sensitive than the current SWIFT satellite, combined with a rapid spectroscopic followup capability.

Distant GRBs have been observed in the NIR from with ground-based telescopes to get spectroscopic redshifts $z \sim 6.7$ and their spectral energy distribution. There are claims for even higher redshift GRBs based on photometric data only. A few of the more frequent lower redshift GRBs have been observed in the optical at a spectral resolution sufficient to identify the strongest ISM lines from intervening gas (i.e. using GRBs as background probes instead of the quasars normally used for this purpose).

c) At high redshift, the 21 cm HI line is shifted to lower frequencies (higher wavelengths) into regimes not normally utilized by radio telescopes. Prototypes for "long wavelength"radio arrays specially designed for the purpose of detecting such emission are being constructed. Since these operate in bands not protected for radio astronomy, there is considerable terrestrial interference and one must go to great lengths to choose a suitable radio-quiet site and then work very hard to reduce the interference even at such a site. The LOFAR (low frequency radio array) is one such project; the central region of Australia, with its very low population density, lack of major cities, etc., is one possible site.

d) For dark matter with certain properties that are predicted by theories of supersymmetry, but have never been observed yet, these particles can self-annihilate to produce ordinary particles such as positrons and neutrinos as well as γ-ray photons. If the Galactic and instrumental backgrounds from long exposures with the Fermi satellite, which is sensitive to

photons with GeV energies, can be very accurately characterized, the it might be possible to detect these energetic photons emitted from regions of high dark matter content. These might include the central region of the Milky Way, nearby dwarf spheroidal galaxies, or dark satellites of the Galaxy (small halos that have been accreted to our galaxy, but never formed stars). If annihilation emission is detected, it will help to characterize the nature of the dark matter.

The possibility of detecting such emission has energized many theoretical studies, but disentangling it from the backgrounds it is very challenging given the expected performance and long-term stability of the Fermi satellite, and may not be possible at all. In addition to the high backgrounds, there are many extragalactic blazars that will be detected as point sources and provide further confusion. There is a major effort at OVRO to identify and monitor such blazars.

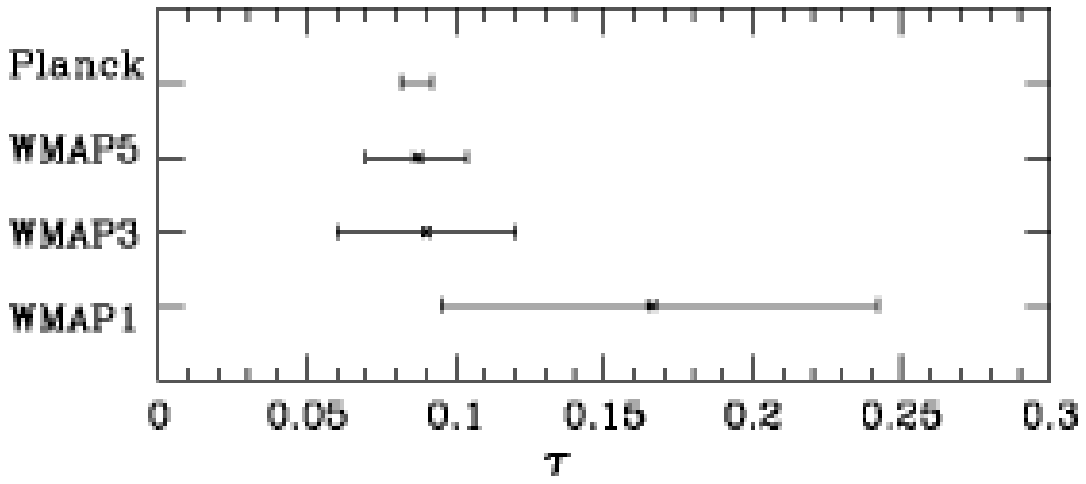

Figure 1. Evolution of WMAP $1-\sigma$ constraints on the optical depth $\tau_{\rm CMB}$ and, for comparison, the predicted error for Planck.

Fig. 10.— Fig. 1 of Pritchard, Loeb & Wyithe (2010), arXiv:0908.3891). They claim that reionization was complete by $z \sim 8$, and that the IGM was 50% ionized at $z = 9$ to 10. The integrated optical depth τ_{CMB} to the surface of last scattering as determined directly from a bump in the CMB power spectrum is shown in the figure. The WMAP 5 year analysis deduces from this that the redshift of reionionization is 11±1.4. This is a direct determination that does not require any model of the IGM, the First Stars, etc.

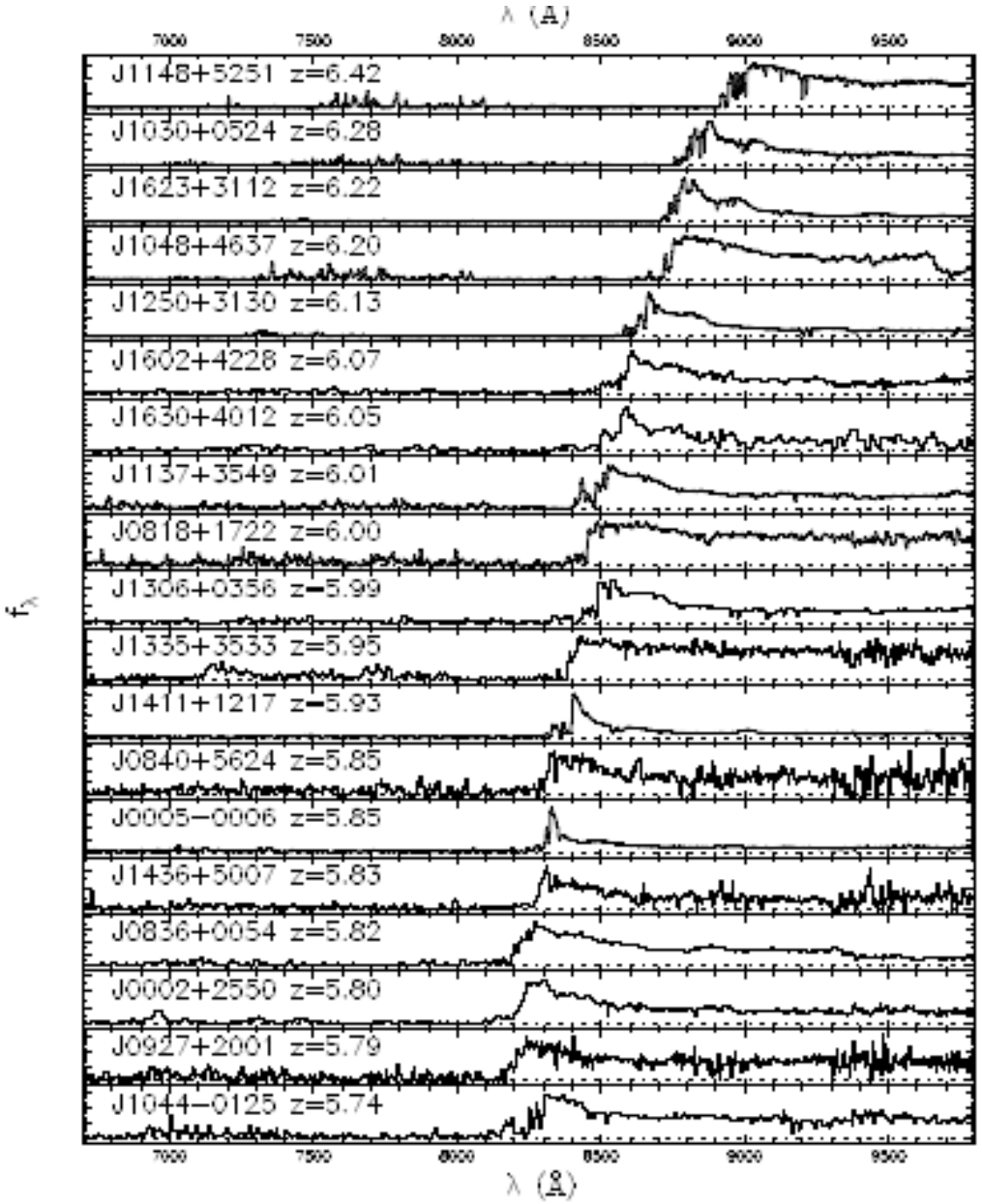

Fig. 1.— Spectra of our sample of nineteen SDSS quasars at $5.74 < z < 6.42$. Twelve of the spectra were taken with Keck/ESI, while the others were observed with the MMT/Red Channel and Kitt Peak 4-meter/MARS spectrographs. See Table 1 for detailed information.

Fig. 11.— Fig. from Fan, Strauss, Richards et al, 2006, ApJ, 131, 1203

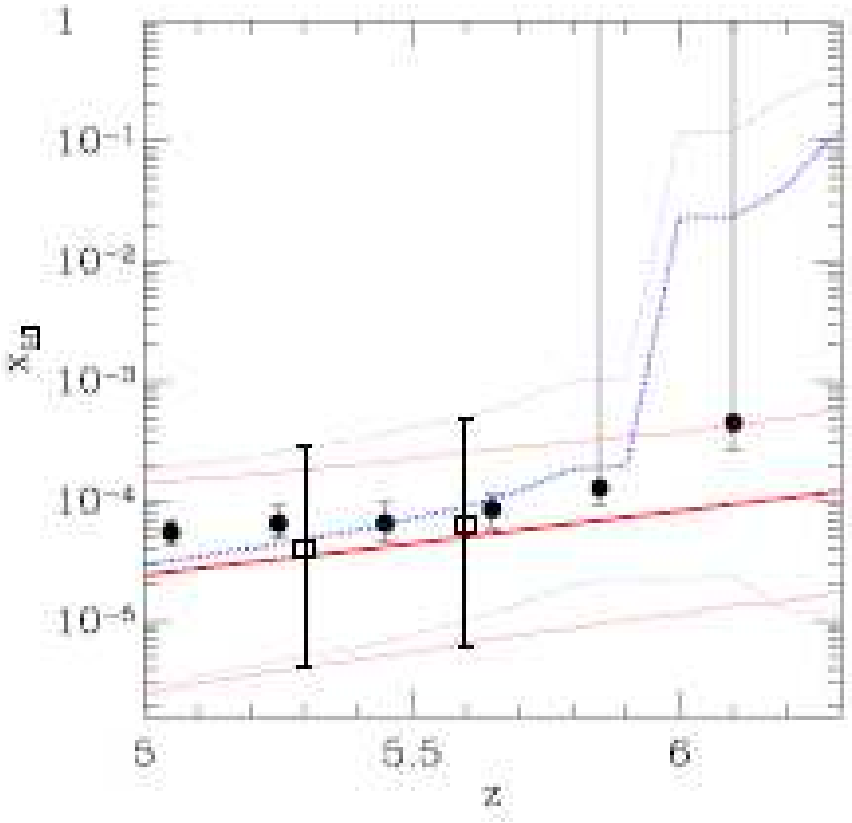

Fig. 1. Evolution of the neutral hydrogen fraction. Thick red solid (blue dotted) lines represent average results over 100 LOS for the ERM (LRM), while the thin lines denote the upper and lower neutral hydrogen fraction extremes in each redshift interval. Solid circles represent x_{HI} estimates by Fan et al. (2006); empty squares denote the results obtained in this work.

Fig. 12.— ERM = early reionization model ending at $z > 7$. Late reionization ending at $z \sim 6$. Fig. 1 of Gallerani, Ferrara, Choudhury et al, 2010.

2

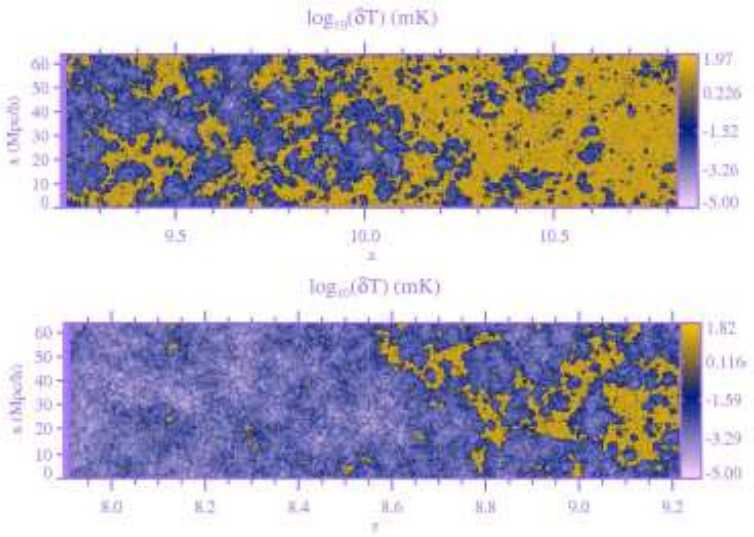

FIG. 1: Simulated maps of the 21 cm background during the early and late stages of a particular reionization scenario (top and bottom panels). Purple regions are highly ionized; yellow regions are mostly neutral. In the vertical direction, the slice subtends $\sim 35'$ on the sky. From [29].

Fig. 13.— Detecting the epoch of reionization via redshifted 21 cm HI. Fig. 1 of Furlanetto et al, Decadal Survey White Paper (Astro-ph:0902.4602), 2010

Direct detection of Pop III (0Z) stars (none detected yet)

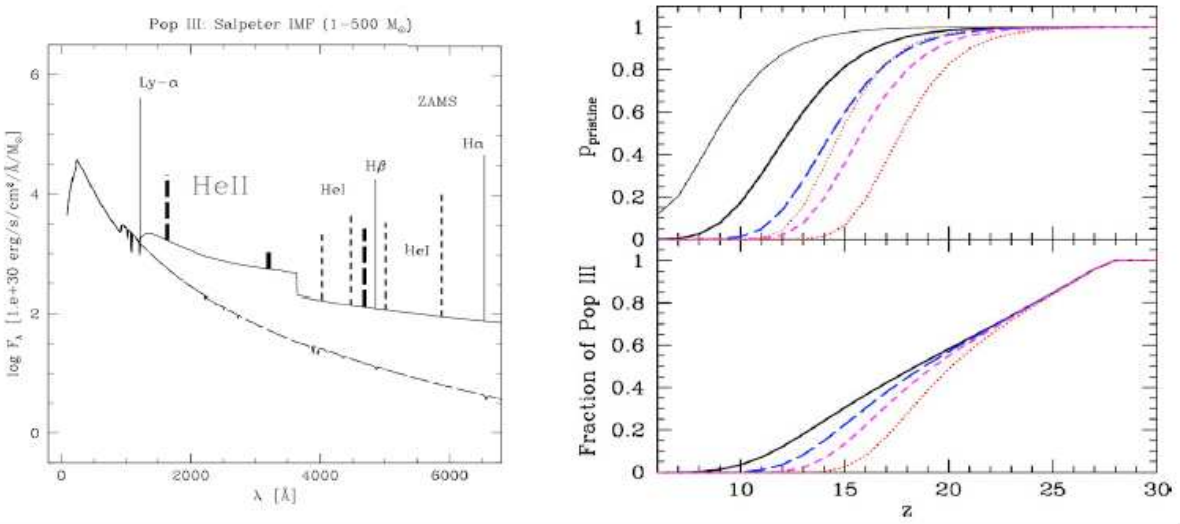

Figure 1. Models of population III star formation. (*Left*) Model spectral energy distributions of massive, metal-free (Population III) stars from Schaerer & Pelló (2002) showing the wealth of signatures of the "hard" radiation field produced by these massive and hot stars. (*Right*) A cosmological model of the contribution of Population III star formation from Furlanetto & Loeb (2005). The top panel shows the fraction of halos that form with metal-free gas for various assumptions, and the bottom panels indicate the fraction of star formation that is Population III, all as a function of redshift.

Fig. 14.— Fig. 1 of Cooke et al, Decadal Survey White Paper (Astro-ph:0902.3674), 2010

Suggestions for student talks:

prospects for observing the 21 cm line at high redshift, what is the predicted flux and how hard will it be to observe this, what will we learn

dark matter annihilation radiation and the Fermi satellite

results thus far from observations of high redshift GRBs.

Suggested reading:

a) First Light, chapter by A. Loeb and by A. Ferrara

b) review of first stars, Bromm & Larson, 2004, ARAA, 42, 79

e) A. Loeb, 2007, "The Frontier of Reionization: Theory and Forthcoming Observations", Astro-ph:0711.3463

f) R. Barkana & A. Loeb, 2001, "In the Beginning: The First Sources of Light and Reionization in the Universe", see Astro-ph:00104683